2014 *IEEE International Conference on Multimedia and Expo* (ICME'14), Chengdu, China, July 2014

HIGH DYNAMIC RANGE IMAGE TONE MAPPING BY OPTIMIZING TONE MAPPED IMAGE QUALITY INDEX

Kede Ma, Hojatollah Yeganeh, Kai Zeng and Zhou Wang

Dept. of Electrical & Computer Engineering, University of Waterloo, Waterloo, ON, Canada
Email: {k29ma, hyeganeh, kzeng, zhou.wang}@uwaterloo.ca

ABSTRACT

An active research topic in recent years is to design tone mapping operators (TMOs) that convert high dynamic range (HDR) to low dynamic range (LDR) images, so that HDR images can be visualized on standard displays. Nevertheless, most existing work has been done in the absence of a well-established and subject-validated image quality assessment (IQA) model, without which fair comparisons and further improvement are difficult. Recently, a tone mapped image quality index (TMQI) was proposed, which has shown to have good correlation with subjective evaluations of tone mapped images. Here we propose a substantially different approach to design TMO, where instead of using any pre-defined systematic computational structure (such as image transformation or contrast/edge enhancement) for tone mapping, we navigate in the space of all images, searching for the image that optimizes TMQI. The navigation involves an iterative process that alternately improves the structural fidelity and statistical naturalness of the resulting image, which are the two fundamental building blocks in TMQI. Experiments demonstrate the superior performance of the proposed method.

Index Terms— tone mapping, tone mapped image quality index (TMQI), high dynamic range imaging, image quality assessment, structural fidelity, statistical naturalness

1. INTRODUCTION

High dynamic range (HDR) images have greater dynamic ranges of intensity levels than standard or low dynamic range (LDR) images, so as to capture the wide luminance variations in real scenes [1]. A problem often encountered in practice is how to visualize HDR images on regular displays which are designed to display LDR images. To overcome this problem, an increasing number of tone mapping operators (TMOs) that convert HDR to LDR images have been developed [1–6]. Because of the reduction in dynamic range, tone mapped images inevitably suffer from information loss, but how to evaluate the quality and information loss of tone mapped images is still an unresolved problem.

Subjective evaluation is the most straightforward quality measure [7–10], but is extremely time consuming, expensive and is difficult to be incorporated into automatic optimization algorithms [11]. Objective quality assessment of tone mapped images is a challenging problem. The original HDR and the tone mapped LDR images have different dynamic ranges, and thus typical objective image quality measures such as peak signal-to-noise ratio (PSNR) and the structural similarity index (SSIM) [11, 12] are not applicable. Little has been done in developing objective methods for HDR images. The HDR visible difference predictor (HDR-VDP) [1, 13] is designed to predict the visibility of distortions between two HDR images of the same dynamic range. A dynamic range independent quality measure was proposed based on HDR-VDP in [14] that produces three quality maps, but does not provide an overall quality score. Recently, a tone mapped image quality index (TMQI) was proposed [15] that measures the quality of an LDR image using its corresponding HDR image as reference. TMQI not only provides an overall quality assessment of a tone mapped image, but also produces a structural fidelity map that indicates how well the local structural details are preserved at each spatial location.

The purpose of this work is to develop a novel TMO that utilizes TMQI as the optimization goal. Unlike existing TMOs, we do not pre-define a computational structure that involves image transformations or gradient/edge estimation and enhancement. Instead, we operate in the space of images, starting from any given point as the initial image and moving our image towards the direction of improving TMQI. Experiments show that this approach leads to consistent enhancement of the perceptual quality of tone mapped images with a wide variety of initial images.

2. TONE MAPPED IMAGE QUALITY INDEX (TMQI)

This section provides a brief background description of the TMQI algorithm proposed in [15]. This is necessary in explaining the TMO method based on TMQI-optimization in Section 3, which is the main contribution of this work. Detailed descriptions of the TMQI algorithm can be found in [15].

Let $\mathbf{X}$ and $\mathbf{Y}$ be the HDR image and the tone mapped LDR image, respectively. The fundamental idea behind TMQI is that a good quality tone mapped image should achieve a good compromise between two key factors – structural fi-

delity and statistical naturalness. The TMQI computation is given by [15]

$$\mathrm{TMQI}(\mathbf{X},\mathbf{Y}) = a[S(\mathbf{X},\mathbf{Y})]^{\alpha} + (1-a)[N(\mathbf{Y})]^{\beta}\,, \quad (1)$$

where S and N denote the structural fidelity and statistical naturalness, respectively. The parameters α and β determine the sensitivities of the two factors, and $0 \le a \le 1$ adjusts the relative importance between them. Both S and N are upper-bounded by 1 and thus TMQI is also upper-bounded by 1.

The computation of the structural fidelity S is patch-based. Let $\mathbf{x}$ and $\mathbf{y}$ be two image patches extracted from $\mathbf{X}$ and $\mathbf{Y}$, respectively. An SSIM-motivated local structural fidelity measure is defined as

$$S_{\mathrm{local}}(\mathbf{x},\mathbf{y}) = \frac{2\tilde{\sigma}_x\tilde{\sigma}_y + C_1}{\tilde{\sigma}_x^2 + \tilde{\sigma}_y^2 + C_1} \cdot \frac{\sigma_{xy} + C_2}{\sigma_x\sigma_y + C_2}\,, \quad (2)$$

where σ_x, σ_y and σ_{xy} denote the local standard deviations and cross correlation between the two corresponding patches, respectively. C_1 and C_2 are stability constants. The first term is a modification of the local contrast comparison component in SSIM [12], and the second term is the same as the structure comparison component in SSIM [12]. The local contrast comparison term is based on two considerations. First, as along as the contrast in the HDR and LDR patches are both significant or both insignificant, the contrast differences should not be penalized. Second, the measure should penalize the cases in which the contrast is significant in one of the patches but not in the other. In TMQI [15], to assess the significance of local contrast, the local standard deviation σ is passed through a nonlinear mapping function given by

$$\tilde{\sigma} = \frac{1}{\sqrt{2\pi}\theta_\sigma}\int_{-\infty}^{\sigma} \exp\left[-\frac{(t-\tau_\sigma)^2}{2\theta_\sigma^2}\right] dt\,, \quad (3)$$

where τ_σ is a contrast threshold and $\theta_\sigma = \tau_\sigma/3$ [15]. The local structural fidelity measure S_{local} is applied using a sliding window that runs across the image, resulting in a map that reflects the variation of structural fidelity across space. Figure 1(f) shows an example of such a structural fidelity map computed for the tone mapped image of Fig. 1(a). Note that due to overexposure, the text details of the brightest book region are missing, which are well indicated in the map. Finally, the quality map is averaged to provide a single overall structural fidelity measure of the image

$$S(\mathbf{X},\mathbf{Y}) = \frac{1}{M}\sum_{i=1}^{M} S_{\mathrm{local}}(\mathbf{x}_i,\mathbf{y}_i)\,, \quad (4)$$

where $\mathbf{x}_i$ and $\mathbf{y}_i$ are the i-th patches in $\mathbf{X}$ and $\mathbf{Y}$, respectively, and M is the total number of patches.

The statistical naturalness model N is derived from the statistics of about 3,000 gray-scale images representing many different types of natural scenes [15]. It was found that the histograms of the mean and standard deviation (std) can be well fitted by a Gaussian density function P_m and a Beta density function P_d, respectively [15]. Based on recent vision science studies on the independence of image brightness and contrast [16], the statistical naturalness is modeled as the product of the two density functions [15]

$$N(\mathbf{Y}) = \frac{1}{K} P_m\, P_d\,, \quad (5)$$

where K is a normalization factor given by $K = \max\{P_m P_d\}$. This constrains the N measure to be bounded between 0 and 1.

3. TONE MAPPING BY OPTIMIZING TMQI

Assuming TMQI to be the quality criterion of tone mapped images, the problem of optimal tone mapping can be formulated as

$$\mathbf{Y}_{\mathrm{opt}} = \arg\max_{\mathbf{Y}} \mathrm{TMQI}(\mathbf{X},\mathbf{Y})\,. \quad (6)$$

This is a challenging problem due to the complexity of TMQI and the high dimensionality (the same as the number of pixels in the image). We propose an iterative algorithm that starts from any initial image $\mathbf{Y}_0$ and searches for the best solution in the image space. Specifically, in each iteration, we first adopt a gradient ascent algorithm to improve the structural fidelity S. We then solve a constrained optimization problem to improve the statistical naturalness N. These two steps are applied alternately until convergence. Details of the algorithm are elaborated as follows.

In the k-th iteration, given the result image $\mathbf{Y}_k$ from the last iteration, a gradient ascent algorithm is first applied to improve the structural fidelity:

$$\hat{\mathbf{Y}}_k = \mathbf{Y}_k + \lambda\, \mathbf{G}_{\mathbf{Y}}|_{\mathbf{Y}=\mathbf{Y}_k}\,, \quad (7)$$

where $\mathbf{G}_{\mathbf{Y}} = \nabla_{\mathbf{Y}} S(\mathbf{X},\mathbf{Y})$ is the gradient of $S(\mathbf{X},\mathbf{Y})$ with respect to $\mathbf{Y}$, and λ controls the updating speed. To compute $\mathbf{G}_{\mathbf{Y}}$, we rewrite the local structural fidelity measure in (2) as

$$S_{\mathrm{local}}(\mathbf{x},\mathbf{y}) = \frac{A_1\, A_2}{B_1\, B_2}\,, \quad (8)$$

where $A_1 = 2\tilde{\sigma}_x\tilde{\sigma}_y + C_1$, $B_1 = \tilde{\sigma}_x^2 + \tilde{\sigma}_y^2 + C_1$, $A_2 = \sigma_{xy} + C_2$, and $B_2 = \sigma_x\sigma_y + C_2$, respectively. Representing both image patches as column vectors of length N_w, we have

$$\mu_y = \frac{1}{N_w}\mathbf{1}^T\mathbf{y} \quad (9)$$

$$\sigma_y^2 = \frac{1}{N_w - 1}(\mathbf{y}-\mu_y)^T(\mathbf{y}-\mu_y) \quad (10)$$

$$\sigma_{xy} = \frac{1}{N_w - 1}(\mathbf{x}-\mu_x)^T(\mathbf{y}-\mu_y)\,. \quad (11)$$

The gradient of local structural fidelity measure with respect to $\mathbf{y}$ can then be expressed as

$$\nabla_{\mathbf{y}} S_{\mathrm{local}}(\mathbf{x},\mathbf{y}) = \frac{(A_1' A_2 + A_1 A_2')}{B_1 B_2} - \frac{(B_1' B_2 + B_1 B_2')A_1 A_2}{(B_1 B_2)^2}\,, \quad (12)$$

where $A_1' = \nabla_{\mathbf{y}} A_1$, $B_1' = \nabla_{\mathbf{y}} B_1$, $A_2' = \nabla_{\mathbf{y}} A_2$, and $B_2' = \nabla_{\mathbf{y}} B_2$, respectively. Noting that $\nabla_{\mathbf{y}} \sigma_y = (\mathbf{y} - \mu_y)/(N_w \sigma_y)$ and $\nabla_{\mathbf{y}} \sigma_{xy} = (\mathbf{x} - \mu_x)/N_w$, we have

$$\begin{aligned} A_1' &= 2\tilde{\sigma}_x \nabla_{\mathbf{y}} \tilde{\sigma}_y \\ &= \frac{2\tilde{\sigma}_x}{\sqrt{2\pi}\theta_\sigma} \exp\left[-\frac{(\sigma_y - \tau_\sigma)^2}{2\theta_\sigma^2}\right] \cdot \nabla_{\mathbf{y}} \sigma_y \\ &= \sqrt{\frac{2}{\pi}} \frac{\tilde{\sigma}_x}{N_w \theta_\sigma \sigma_y} \exp\left[-\frac{(\sigma_y - \tau_\sigma)^2}{2\theta_\sigma^2}\right] (\mathbf{y} - \mu_y) \quad (13) \\ B_1' &= 2\tilde{\sigma}_y \nabla_{\mathbf{y}} \tilde{\sigma}_y \\ &= \sqrt{\frac{2}{\pi}} \frac{\tilde{\sigma}_y}{N_w \theta_\sigma \sigma_y} \exp\left[-\frac{(\sigma_y - \tau_\sigma)^2}{2\theta_\sigma^2}\right] (\mathbf{y} - \mu_y) \quad (14) \\ A_2' &= \frac{1}{N_w}(\mathbf{x} - \mu_x) \quad (15) \\ B_2' &= \sigma_x \nabla_{\mathbf{y}} \sigma_y = \frac{\sigma_x}{N_w \sigma_y}(\mathbf{y} - \mu_y)\,. \quad (16) \end{aligned}$$

Plugging (13), (14), (15) and (16) into (12), we obtain the gradient of local structural fidelity. Finally, the gradient of the global structural fidelity is given by

$$\mathbf{G}_{\mathbf{Y}} = \nabla_{\mathbf{Y}} S(\mathbf{X}, \mathbf{Y}) = \frac{1}{M} \sum_{i=1}^{M} \mathbf{R}_i^T \nabla_{\mathbf{y}} S_{\text{local}}(\mathbf{x}_i, \mathbf{y}_i)\,, \quad (17)$$

where $\mathbf{x}_i = \mathbf{R}_i(\mathbf{X})$ and $\mathbf{y}_i = \mathbf{R}_i(\mathbf{Y})$ are the i-th image patches, $\mathbf{R}_i$ is the operator that takes the i-th local patch from the image, and $\mathbf{R}_i^T$ places the patch back into the corresponding location in the image.

After the structural fidelity update step of (7), we obtain an intermediate image $\hat{\mathbf{Y}}_k$, which will be further updated to $\mathbf{Y}_{k+1}$ such that the statistical naturalness is improved. This is done by a point-wise intensity transformation through a three-segment equipartition monotonic piecewise linear function given by

$$y_{k+1}^i = \begin{cases} (3/L) a \hat{y}_k^i & 0 \le \hat{y}_k^i \le L/3 \\ (3/L)(b-a)\hat{y}_k^i + (2a - b) & L/3 < \hat{y}_k^i \le 2L/3 \\ (3/L)(L-b)\hat{y}_k^i + (3b - 2L) & 2L/3 < \hat{y}_k^i \le L \end{cases} \quad (18)$$

where L is the dynamic range of the tone mapped images, and the parameters a and b (where $0 \le a \le b \le L$) need to be selected so that the mapped image $\mathbf{Y}_{k+1} = \{y_{k+1}^i \text{ for all } i\}$ has increased likelihood of mean μ_{k+1} and std σ_{k+1} values based on the statistical naturalness models P_m and P_d described in Section 2. To solve for a and b, we first decide on the desired mean and std values by

$$\begin{aligned} \mu_{k+1}^d &= \hat{\mu}_k + \lambda_m (c_{P_m} - \hat{\mu}_k) \\ \sigma_{k+1}^d &= \hat{\sigma}_k + \lambda_d (c_{P_d} - \hat{\sigma}_k)\,, \end{aligned} \quad (19)$$

where $\hat{\mu}_k$ and $\hat{\sigma}_k$ are the mean and std of $\hat{\mathbf{Y}}_k$, respectively. c_{P_m} and c_{P_d} are the values corresponding to the peaks in the P_m and P_d models, respectively. λ_m and λ_d are step sizes that controls the updating speed. As such, finding the parameters a and b can be formulated as an optimization problem

$$\begin{aligned} \{a, b\}_{\text{opt}} = \underset{\{a,b\}}{\arg\min} &||\mu_{k+1} - \mu_{k+1}^d||^2 + \eta ||\sigma_{k+1} - \sigma_{k+1}^d||^2 \\ &\text{subject to } 0 \le a \le b \le L\,, \end{aligned} \quad (20)$$

where η controls the relative importance between the mean and std terms. In our implementation, Matlab function *fmincon* with interior-point algorithm is used to solve this optimization problem. Once the optimal values of a and b are obtained, they are plugged into (18) to create the output image $\mathbf{Y}_{k+1}$, which is subsequently employed as the input image in the $(k+1)$-th iteration.

The iteration continues until convergence, which is determined by checking the difference between the images of consecutive iterations. Specifically, when $||\mathbf{Y}_{k+1} - \mathbf{Y}_k|| < \epsilon$, the iteration stops. The proposed algorithm involves totally five parameters, which are set empirically to $\epsilon = 0.01$, $\lambda = 0.3$, $\lambda_m = \lambda_d = 0.03$ and $\eta = 1$ in all of our experiments.

4. EXPERIMENTAL RESULTS

The proposed algorithm is tested on a database of 14 HDR images, which include various contents such as humans, landscapes, architectures, as well as indoor and night scenes [15]. Due to space limit, only partial results are presented here, but similar performance is observed throughout the database.

We first examine the roles of the structural fidelity and statistical naturalness components separately. In Fig. 1, we start with an initial "desk" image created by Reinhard's TMO [2] (one of the best TMOs based on several independent subjective tests [9, 15]), and then apply the proposed iterative algorithm but using structural fidelity updates only. It can be observed that the structural fidelity map is very effective at detecting the missing structures (e.g., text in the book region, and fine textures on the desk), and the proposed algorithm successfully recovers such structures after a sufficient number of iterations. The improvement of structure details is also well reflected by the structural fidelity maps, which eventually evolve to a nearly uniform white image. By contrast, in Fig. 2, the initial "building" image is created by a Gamma correction mapping ($\gamma = 2.2$), and we apply the proposed iterative algorithm but using statistical naturalness updates only. With the iterations, the overall brightness and contrast of the image are significantly improved, leading to a more visually appealing and natural-looking image.

The results shown in Figs. 3 and 4 are obtained by applying the full proposed algorithm. In Fig. 3, the initial images are created by Reinhard's TMO [2]. Although the initial image of Fig. 3(a) has a seemingly reasonable visual appearance, the fine details of the woods, the brick textures of the tower, and the details in the clouds are fuzzy or invisible. The proposed algorithm recovers these fine details and makes them much sharper, as can be seen in Fig. 3(b). In addition, the

(a) initial image (b) after 10 iterations (c) after 50 iterations (d) after 100 iterations (e) after 200 iterations

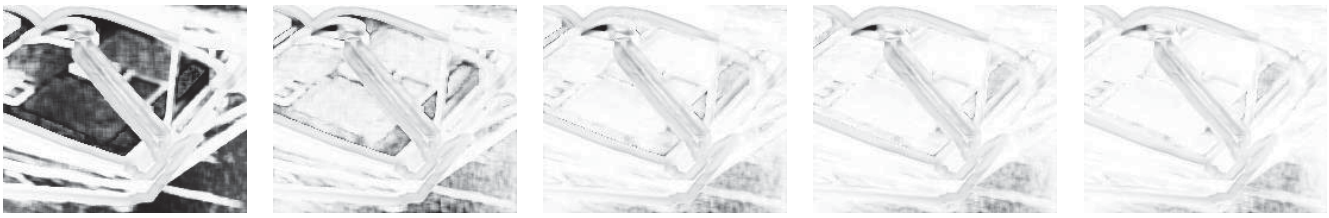

(f) initial image, S = 0.689 (g) 10 iterations, S = 0.921 (h) 50 iterations, S = 0.954 (i) 100 iterations, S = 0.961 (j) 200 iterations, S = 0.966

Fig. 1. Tone mapped "desk" images and their structural fidelity maps. (a): initial image created by Reinhard's algorithm [2]; (b)-(e): images created using iterative structural fidelity update only; (f)-(j): corresponding structural fidelity maps of (a)-(e), where brighter indicates higher structural fidelity. All images are cropped for better visulization.

(a) initial image, N = 0.000 (b) 10 iterations, N = 0.001 (c) 50 iterations, N = 0.428 (d) 100 iterations, N = 0.868 (e) 200 iterations, N = 0.971

Fig. 2. Tone mapped "building" images. (a): initial image created by Gamma correction ($\gamma = 2.2$); (b)-(e): images created using iterative statistical naturalness update only.

(a) S=0.847, N = 0.746 (b) S=0.971, N = 1.000 (c) S=0.787, N = 0.966 (d) S=0.970, N = 0.999

Fig. 3. Tone mapped "bridge" and "lamp" images. (a) and (c): initial images created by Reinhard's algorithm [2]; (b) and (d): images after applying the proposed algorithm.

(a) S=0.148, N=0.000 (b) S=0.959, N=0.997 (c) S=0.521, N=0.038 (d) S=0.976, N=0.999

Fig. 4. Tone mapped "memorial" and "woman" images. (a) and (c): initial images created by Gamma correction; (b) and (d): images after applying the proposed algorithm.

overall appearance is more pleasant due to statistical naturalness update. Similar results are also observed in Fig. 3(d), where the details on the wall, scribbling papers and the drawer are well recovered. In Fig. 4, the initial images are obtained by applying Gamma correction mapping ($\gamma = 2.2$), which creates dark images with missing details. Starting from these images, the proposed iterative algorithm successfully recovers most details in the images and presents more realistic and pleasant appearance. It is worth mentioning that the proposed method often recovers image details that are unseen in the initial images, for example, the wall and door in the background are missing in Fig. 4(c) but are clearly visible in Fig. 4(d).

We test the proposed method not only on various images with different contents, but also using initial images generated by a variety of TMOs. Due to space limit, only partial results are reported in Table 1, where it can be seen that the proposed algorithm consistently converges to images with both high structural fidelity and high statistical naturalness, which produces high TMQI values even when the initial images are created by the most competitive state-of-the-art TMOs.

To have a close look at the iterative behavior of the proposed method, Figs. 5 and 6 show the structural fidelity and statistical naturalness measures as functions of iteration using different initial images as the starting point. There are several useful observations. First, both measures increase monotonically with iterations. Second, the proposed algorithm converges in all cases regardless using simple or sophisticated TMO results as initial images. Third, different initial images may result in different converged images. From these observations, we conclude that the proposed iterative algorithm is well behaved, but the high-dimensional search space is complex and contains many local optima, and the proposed algorithm may be trapped in one of the local optima.

The computation complexity of the proposed algorithm increases linearly with the number of pixels in the image. Our unoptimized Matlab implementation takes around 4 seconds per iteration for a 341×512 image on an Intel Quad-Core 2.67 GHz computer.

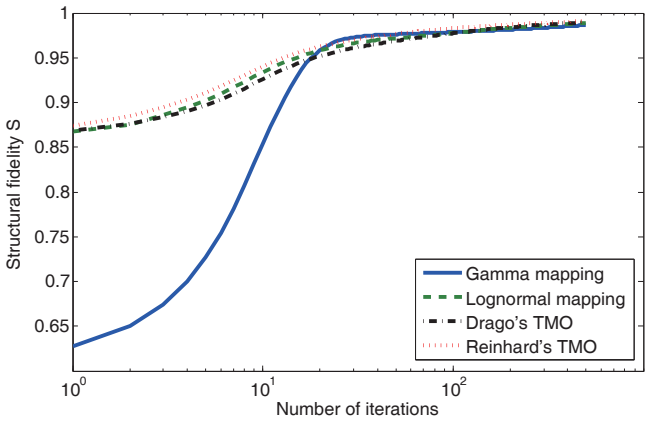

Fig. 5. Structural fidelity as a function of iteration with initial "woods" images created by different TMOs.

5. CONCLUSIONS AND DISCUSSIONS

We propose a novel approach to design TMOs by navigating in the space of images to find the optimal image in terms of TMQI. The navigation is based on an iterative approach that alternates between improving the structural fidelity preservation and enhancing the statistical naturalness of the image. Experimental results show that both steps contribute significantly to the improvement of the overall quality of the tone mapped image. Our experiments also show that the proposed method is well behaved, and effectively enhances the image

Table 1. TMQI comparison between initial and converged images

Image		Gamma mapping	Reinhard [2]	Drago [3]	Lognormal mapping
Bridge	initial image	0.8093	0.9232	0.8848	0.7439
	converged image	0.9928	0.9929	0.9938	0.9944
Lamp	initial image	0.5006	0.9387	0.8717	0.7371
	converged image	0.9906	0.9925	0.9910	0.9894
Memorial	initial image	0.4482	0.9138	0.8685	0.7815
	converged image	0.9895	0.9894	0.9868	0.9867
Woman	initial image	0.6764	0.8891	0.8918	0.8026
	converged image	0.9941	0.9947	0.9943	0.9937

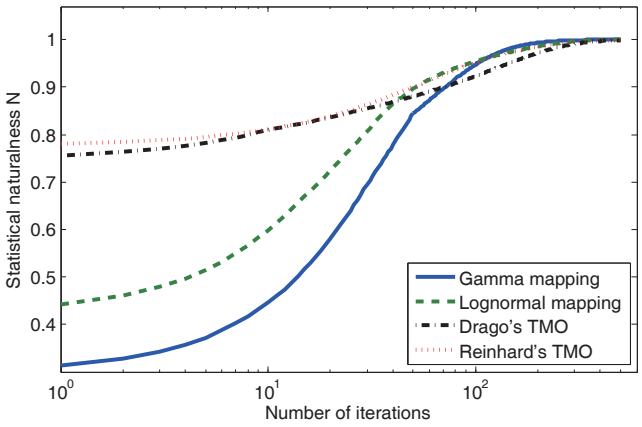

Fig. 6. Statistical naturalness as a function of iteration with initial "woods" images created by different TMOs.

quality from a wide variety of initial images, including those created from state-of-the-art TMOs.

The current work opens the door to a new class of TMO approaches. Many topics are worth further investigations. First, as is the case for any algorithm operating in complex high-dimensional space, the current approach only finds local optima. Deeper understanding of the search space is desirable. Second, the current implementation is computationally costly and requires a large number of iterations to converge. Fast search algorithms are necessary to accelerate the iterations. Third, the current statistical naturalness model is rather crude. Incorporating advanced models of image naturalness into the proposed framework has great potentials in creating more natural-looking tone mapped images.

6. REFERENCES

[1] E. Reinhard, W. Heidrich, P. Debevec, S. Pattanaik, G. Ward, and K. Myszkowski, *High Dynamic Range Imaging: Acquisition, Display, and Image-based Lighting*. Morgan Kaufmann, 2010.

[2] E. Reinhard, M. Stark, P. Shirley, and J. Ferwerda, "Photographic tone reproduction for digital images," *ACM TOG*, vol. 21, no. 3, pp. 267–276, 2002.

[3] F. Drago, K. Myszkowski, T. Annen, and N. Chiba, "Adaptive logarithmic mapping for displaying high contrast scenes," *Computer Graphics Forum*, vol. 22, pp. 419–426, 2003.

[4] R. Fattal, D. Lischinski, and M. Werman, "Gradient domain high dynamic range compression," *ACM TOG*, vol. 21, no. 3, pp. 249–256, 2002.

[5] Y. Salih, A. S. Malik, N. Saad, *et al.*, "Tone mapping of hdr images: A review," in *IEEE ICIAS*, vol. 1, pp. 368–373, 2012.

[6] H. Yeganeh and Z. Wang, "High dynamic range image tone mapping by maximizing a structural fidelity measure," in *IEEE ICASSP*, pp. 1879–1883, 2013.

[7] F. Drago, W. L. Martens, K. Myszkowski, and H.-P. Seidel, "Perceptual evaluation of tone mapping operators," in *ACM SIGGRAPH Sketches & Applications*, 2003.

[8] M. Čadík and P. Slavik, "The naturalness of reproduced high dynamic range images," in *IEEE International Conference on Information Visualisation*, pp. 920–925, 2005.

[9] M. Čadík, M. Wimmer, L. Neumann, and A. Artusi, "Evaluation of hdr tone mapping methods using essential perceptual attributes," *Computers & Graphics*, vol. 32, no. 3, pp. 330–349, 2008.

[10] C. Cavaro-Ménard, L. Zhang, and P. Le Callet, "Diagnostic quality assessment of medical images: Challenges and trends," in *2nd European Workshop on Visual Information Processing*, pp. 277–284, 2010.

[11] Z. Wang and A. C. Bovik, "Mean squared error: Love it or leave it? A new look at signal fidelity measures," *IEEE SPM*, vol. 26, pp. 98–117, Jan. 2009.

[12] Z. Wang, A. C. Bovik, H. R. Sheikh, and E. P. Simoncelli, "Image quality assessment: From error visibility to structural similarity," *IEEE TIP*, vol. 13, pp. 600–612, Apr. 2004.

[13] R. Mantiuk, S. J. Daly, K. Myszkowski, and H.-P. Seidel, "Predicting visible differences in high dynamic range images: model and its calibration," in *Proc. SPIE*, vol. 5666, pp. 204–214, 2005.

[14] T. O. Aydin, R. Mantiuk, K. Myszkowski, and H.-P. Seidel, "Dynamic range independent image quality assessment," *ACM TOG*, vol. 27, no. 3, p. 69, 2008.

[15] H. Yeganeh and Z. Wang, "Objective quality assessment of tone-mapped images," *IEEE TIP*, vol. 22, no. 2, pp. 657–667, 2013.

[16] V. Mante, R. A. Frazor, V. Bonin, W. S. Geisler, and M. Carandini, "Independence of luminance and contrast in natural scenes and in the early visual system," *Nature neuroscience*, vol. 8, no. 12, pp. 1690–1697, 2005.